

Thermal- and Light-Induced Spin-Crossover Characteristics of a Functional Iron(II) Complex at Submonolayer Coverage on HOPG

Sangeeta Thakur,* Evangelos Golias, Ivar Kumberg, Kuppasamy Senthil Kumar,* Rahil Hosseinifar, Jorge Torres-Rodríguez, Lalminthang Kipgen, Christian Lotze, Lucas M. Arruda, Chen Luo, Florin Radu, Mario Ruben,* and Wolfgang Kuch*

Cite This: *J. Phys. Chem. C* 2021, 125, 13925–13932

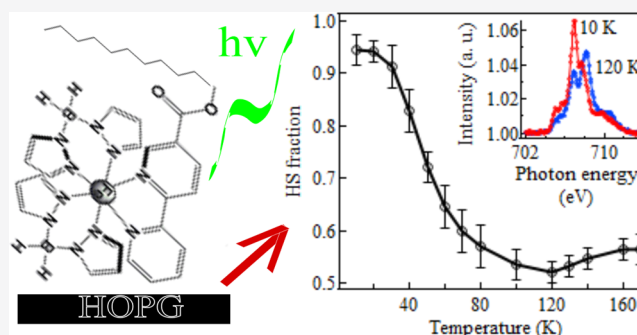
Read Online

ACCESS |

Metrics & More

Article Recommendations

ABSTRACT: Studies on the spin-state switching characteristics of surface-bound thin films of spin-crossover (SCO) complexes are of interest to harness the device utility of the SCO complexes. Molecule–substrate interactions govern the SCO of surface-bound films in direct contact with the underlying substrates. In this study, we elucidate the role of molecule–substrate interactions on the thermal- and light-induced spin-state switching characteristics of a functional SCO-complex— $[\text{Fe}(\text{H}_2\text{B}(\text{pz})_2)_2\text{COOC}_{12}\text{H}_{25}\text{-bipy}]$ (pz = pyrazole, $\text{C}_{12}\text{-bpy}$ = dodecyl[2,2'-bipyridine]-5-carboxylate) deposited at a submonolayer coverage on a highly oriented pyrolytic graphite (HOPG) substrate. A spin-state coexistence of 42% low-spin (LS) and 58% high-spin (HS) is observed for the 0.4 ML deposit of the complex at 40 K, in contrast to the complete spin-state switching observed in the bulk and in SiO_x -bound 10 nm thick films. Cooling the sample to 10 K results in a decrease of the LS fraction to 36%, attributed to soft-X-ray-induced excited spin-state trapping (SOXIESST). Illumination of the sample with a green light ($\lambda = 520 \text{ nm}$) at 10 K caused the LS-to-HS switching of the remaining (36%) LS complexes, by a process termed light-induced excited spin-state trapping (LIESST). The mixed spin-state in the submonolayer coverage of $[\text{Fe}(\text{H}_2\text{B}(\text{pz})_2)_2\text{COOC}_{12}\text{H}_{25}\text{-bipy}]$ highlights the role of molecule–HOPG substrate interactions in tuning the thermal SCO characteristics of the complex. The 100% HS state obtained after light irradiation indicates the occurrence of efficient on-surface light-induced spin switching, encouraging the development of light-addressable molecular devices based on SCO complexes.



INTRODUCTION

SCO molecular complexes undergo reversible LS-to-HS switching and vice versa upon application of an external stimulus such as temperature, light, electric field, or pressure.^{1–8} Spin-state switching of SCO complexes is studied in thin films on different substrates to progress toward applications such as spintronic devices and molecular electronics.^{9–13} Vacuum sublimation is a suitable technique for the fabrication of ultraclean spin-state-switchable thin films, and the SCO characteristics of a range of sublimable SCO complexes have been studied for coverages ranging from submonolayer to multilayer thin films (10 ML).^{2–5,14–16} A clear difference between the SCO characteristics in the bulk and thin films has been observed, especially in few-layer SCO films. Such differences are pronounced for films deposited on metallic substrates due to strong metal–SCO molecule interactions.¹⁵

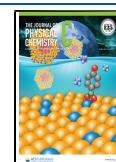
Fragmentation of molecules is commonly observed in SCO complexes in direct contact with a metallic substrate such as Au(111); the remaining undissociated molecules either

undergo spin-state switching or remain trapped in the LS or HS state.^{6,14,17–19} Avoidance of fragmentation and a complete spin-state switching have been observed for some SCO complexes deposited on semimetal and HOPG substrates.^{2–6} The study of SCO on HOPG is especially interesting, because HOPG is an ideal mimic of graphene and features metal-like electrical conductivity, rendering HOPG-bound SCO complexes potentially suitable for device applications. There have been several reports on the efficient thermal- and light-induced spin switching characteristics of Fe(II) complexes deposited on HOPG, elucidating the possible utility of thin SCO-complex deposits as light- and temperature-addressable molecular device architectures.^{2–6,20}

Received: March 30, 2021

Revised: June 4, 2021

Published: June 21, 2021



While the role of the substrate in tuning the SCO of surface-bound films is well established, the nature of intermolecular interactions in surface-bound films remains challenging to control.²² Such control is desirable, considering the pivotal role of intermolecular interactions in governing the SCO in bulk crystalline samples.²³ Intermolecular interactions in thin sublimed films are often different from the ones observed in the bulk samples, which results in different switching characteristics of thin surface-bound films and bulk samples of the same molecule. In a recent report, Ruben and co-workers have shown that a molecular self-assembly strategy could be adopted to obtain similar SCO characteristics in the bulk and thin films of a functional and sublimable SCO complex $[\text{Fe}(\text{H}_2\text{B}(\text{pz})_2)_2\text{COOC}_{12}\text{H}_{25}\text{-bipy}]$.²¹ Figure 1a shows the

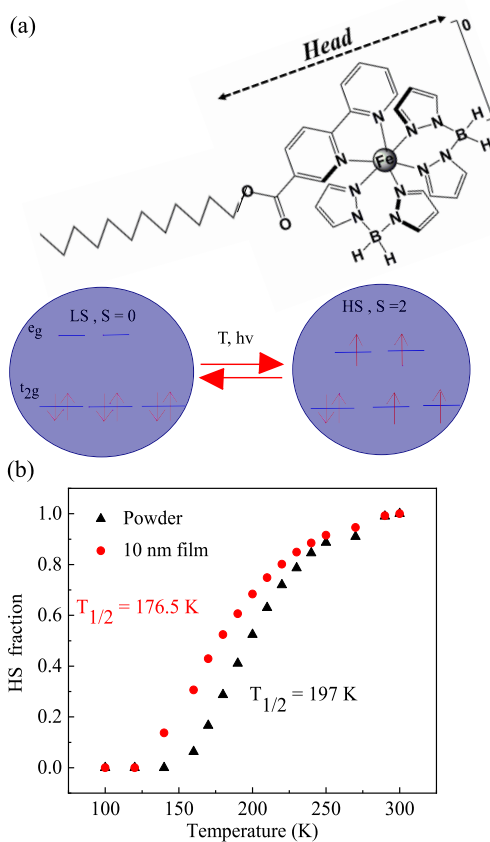


Figure 1. (a) Molecular structure of the $[\text{Fe}(\text{H}_2\text{B}(\text{pz})_2)_2\text{COOC}_{12}\text{H}_{25}\text{-bipy}]$ complex and a schematic representation of spin-state switching in $d^6\text{-Fe}(\text{II})$ SCO complexes. (b) Temperature dependence of the HS fraction of the complex in the bulk and 10 nm thin films, obtained from XAS studies.²¹ (Reproduced with permission from ref 21, copyright John-Wiley and Sons.)

molecular structure of $[\text{Fe}(\text{H}_2\text{B}(\text{pz})_2)_2\text{COOC}_{12}\text{H}_{25}\text{-bipy}]$ and a schematic representation of the HS, LS state of 3d orbital electronic contribution in d^6 SCO complexes.⁵ Figure 1b demonstrates the similar spin-state-switching characteristics in the bulk and in a thin film.²¹ The hydrophobic alkyl chains (Figure 1) in $[\text{Fe}(\text{H}_2\text{B}(\text{pz})_2)_2\text{COOC}_{12}\text{H}_{25}\text{-bipy}]$ can also impart hydrophobic interactions when deposited on a carbonaceous substrate such as HOPG. Thus, $[\text{Fe}(\text{H}_2\text{B}(\text{pz})_2)_2\text{COOC}_{12}\text{H}_{25}\text{-bipy}]$ is ideally suited to study the role of molecule–surface hydrophobic interactions in tuning the SCO properties. To the best of our knowledge, the role of

hydrophobic interactions of functional SCO molecules in direct contact with a carbonaceous substrate such as HOPG is yet to be studied. In this study, we report on the thermal- and light-induced SCO characteristics of HOPG-bound $[\text{Fe}(\text{H}_2\text{B}(\text{pz})_2)_2\text{COOC}_{12}\text{H}_{25}\text{-bipy}]$ at submonolayer coverage using X-ray absorption spectroscopy (XAS) measurements. The sensitivity of XAS to the spin-state of an iron(II) complex renders the method suitable to study SCO complexes deposited on surfaces at submonolayer coverages. Intensity variations of the Fe $L_{2,3}$ edges, following spin-state switching, allow the quantification of LS and HS states, as a function of temperature and light-irradiation time.^{2,4} Ex-situ atomic force microscopy (AFM) measurements have also been performed to get insights into the morphology of the submonolayer deposits on the HOPG surface.

EXPERIMENTAL SECTION

HOPG with dimensions $12 \times 12 \times 2 \text{ mm}^3$ was purchased from tectra GmbH Physikalische Instrumente. The substrate was cleaved at a pressure of 10^{-7} mbar by carbon tape to obtain a clean surface. The molecular powder is evaporated from a tantalum Knudsen cell at 373 K at a pressure of 2×10^{-9} mbar. A submonolayer of $[\text{Fe}(\text{H}_2\text{B}(\text{pz})_2)_2\text{COOC}_{12}\text{H}_{25}\text{-bipy}]$ was deposited on the HOPG substrate held at a temperature of ≈ 250 K. XAS measurements were performed at the VEKMAG endstation of the beamline PM2 of the synchrotron radiation facility BESSY II of the Helmholtz-Zentrum Berlin at a pressure of about 5×10^{-10} mbar. XAS measurements were acquired in total-electron-yield mode by recording the sample drain current as a function of photon energy. The photon flux density is estimated to be $\approx 5 \times 10^9$ photons $\text{s}^{-1} \text{ mm}^{-2}$. The XAS signal was normalized to the one of the Pt grid in the PM2-VEKMAG²⁴ upstream to the experiment and to the background signal from a clean HOPG substrate. The Fe $L_{2,3}$ -edge XAS measurements were recorded at the magic angle of 54.7° between the X-ray wavevector and the surface normal using p-polarized X-rays. At the magic angle, the XAS resonance intensities are independent from the orientation of the molecular orbitals.²⁵ The measurements involving light-induced effects at low temperature were performed with a green LED of $\lambda = 520$ nm with a spectral width (fwhm) of 30 nm. The flux density at the sample position is estimated to be $4.2(8) \times 10^{14}$ photons $\text{s}^{-1} \text{ mm}^{-2}$. The details of the optical setup have been described elsewhere.² AFM measurements are carried out ex situ in ambient conditions in a commercial Nanotec Cervantes AFM system in tapping mode using a Si cantilever of stiffness 2.7 N/m with a resonance frequency of 75 kHz. A thin film of 0.4 ML coverage was prepared under similar conditions as described for the XAS experiments and the sample transferred to air for AFM measurements.

To study the on-surface spin-state switching of $[\text{Fe}(\text{H}_2\text{B}(\text{pz})_2)_2\text{COOC}_{12}\text{H}_{25}\text{-bipy}]$, 0.4 ML of the complex was deposited on a freshly cleaved HOPG surface held at 250 K in the preparation chamber. Then the substrate was transferred under vacuum to the characterization chamber, where the manipulator was kept at 10 K. The transfer rod connecting the two chambers was at room temperature (RT). For transfer and adjustment, the sample was illuminated by standard white LED-based spotlights. All this takes approximately 20 min, while the sample remains at 10 K. The coverage is determined by comparing the Fe L_3 peak intensity with earlier published work on similar Fe(II) spin-crossover molecules on HOPG; for details, see ref 19. In short, the Fe XA signal has been

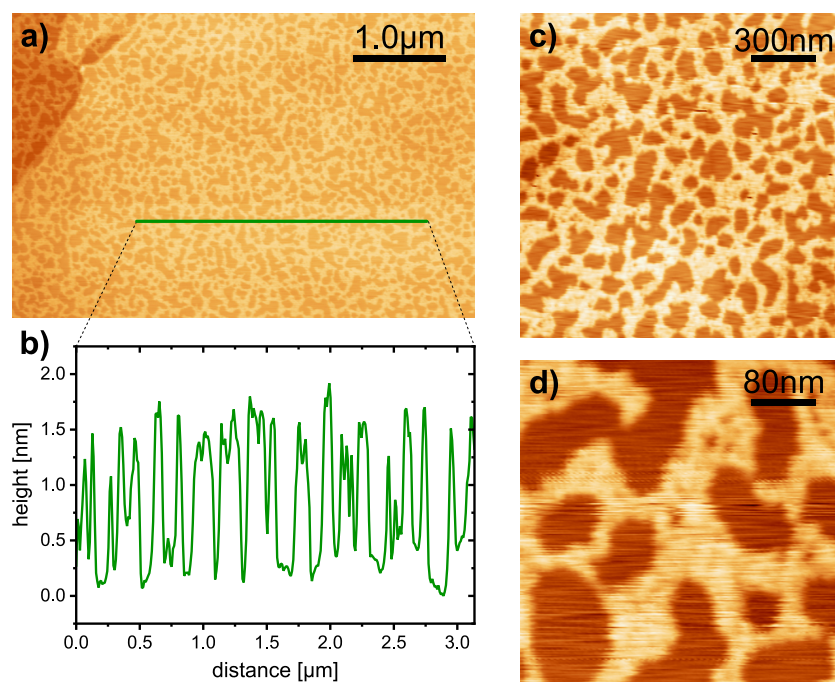


Figure 2. (a) AFM topography image of 0.4 ML of the $[\text{Fe}(\text{H}_2\text{B}(\text{pz})_2)_2\text{COOC}_{12}\text{H}_{25}\text{-bipy}]$ complex on HOPG, (b) line scan across the molecular island along the green line in (a), and (c, d) zoomed in views of (a) showing the molecular layer.

calibrated to a Fe octaethyl–porphyrin (Cl)/Cu(001) reference sample, the coverage of which has been determined by scanning tunneling microscopy, while considering the different XA intensity ratio of HOPG and Cu(001) in the pre-edge region of the Fe L_3 edge.

For the temperature-dependent measurements, the sweeping rate of the temperature was around 4 K in 2–4 min during heating of the sample, while cooling down it was around 4 K in 2–7 min (2 min at higher, 7 min at lower temperatures). XAS spectra were taken after the stabilization of the temperature at a particular value. It took around 3 min to measure an XAS spectrum of the Fe L_3 edge. To quantify the HS fraction, XAS spectra were fitted by a linear combination of a pure HS spectrum at 300 K and a pure LS spectrum at 10 K, which were taken from an earlier study on the parent molecule³ $[\text{Fe}(\text{H}_2\text{B}(\text{pz})_2)_2\text{-bipy}]$, because the present molecule did not show a complete LS state at 10 K. The fitting was done by varying the value of the HS fraction and the error bar represents values of the HS fraction resulting in equally good fits. The value of the LS fraction is determined by subtracting the HS fraction obtained by fitting the spectrum from the value of the HS fraction obtained at 300 K.

RESULTS AND DISCUSSION

In Figure 2a an AFM topography image of 0.4 ML of $[\text{Fe}(\text{H}_2\text{B}(\text{pz})_2)_2\text{COOC}_{12}\text{H}_{25}\text{-bipy}]$ on HOPG is shown. The molecules form nanoporous islands on the HOPG substrate similar to the structure of a submonolayer of $[\text{Fe}(\text{H}_2\text{B}(\text{pz})_2)_2\text{-phen}]$ or $[\text{Fe}(\text{H}_2\text{B}(\text{pz})_2)_2\text{-bipy}]$ on the same surface.^{2,5} The arrangement of the molecules in nanoporous islands is highlighted in panels c and d of Figure 2 using a higher magnification. The average height of the islands is about 1.2 nm (Figure 2b), which matches the height of a single molecule.²⁶ We can conclude that the complexes are forming a molecular layer and virtually all the molecules are in contact

with the surface, but the morphology of the molecular islands in vacuum may be different.

In order to disentangle the influences of temperature change and light illumination on the switching behavior, we performed three sets of XAS experiments. First, purely thermal switching is studied by consecutive heating and cooling cycles with only X-rays present. In the second set, we investigated the effect of green-light illumination with time at a fixed temperature. Lastly, to separate the effects of temperature and illumination clearly, we measured heating and cooling cycles under constant illumination to quantify the kinetics in terms of HS-LS switching rates.

Figure 3a shows Fe $L_{2,3}$ -edge spectra taken at 10 K after transfer to the characterization chamber (as-prepared) and at 300 K. The measurement at 300 K was done after heating the sample from 10 to 300 K. An intense peak around 706.9 eV and a small shoulder around 707.7 eV of the Fe L_3 edge indicate the HS state of the film at 10 K.^{2,4,21} Remarkably, the HS state of the film at 10 K is in stark contrast to the LS state of the bulk complex at 10 K.²¹ Light-induced excited spin-state trapping (LIESST)²⁷ and soft-X-ray-induced excited spin-state trapping (SOXIESST)²⁸ could have contributed to the formation of the HS state of the film at 10 K. The LIESST phenomenon arises due to electron transfer from the LS state to an MLCT (metal-to-ligand charge transfer) state, which then relaxes via intermediate states to the HS state.²⁷ A partial LIESST-induced LS-to-HS switching could have happened due to unavoidable exposure to light during the sample transfer onto the manipulator of the characterization chamber.

The branching ratio^{29,30} $\frac{I_3}{(I_3 + I_2)}$, where I_x is the integrated intensity at the corresponding L_x edge, was evaluated at 10 K (as prepared) and at 300 K. The branching ratio evaluates to 0.51(3) at 10 K and 0.47(3) at 300 K. The intensity differences between the HS spectrum at room temperature and at 10 K as prepared might be attributed to the different thermal

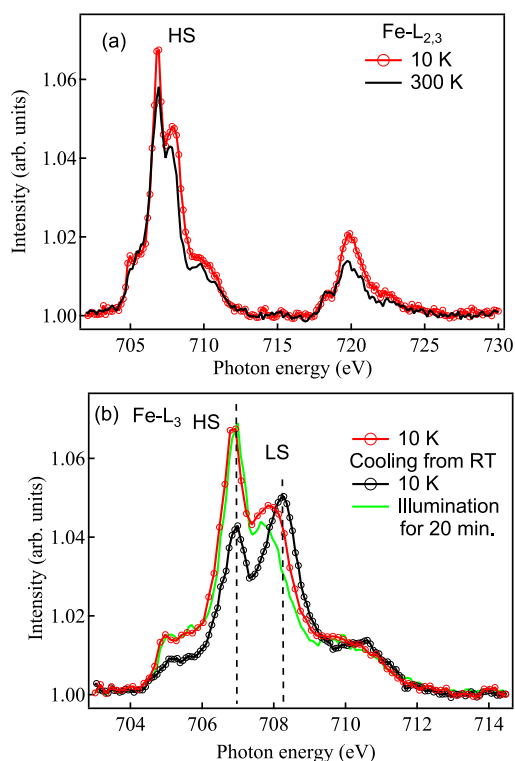


Figure 3. (a) Fe $L_{2,3}$ -edge spectra of the as-prepared sample at 10 K and after heating the sample to 300 K. (b) Comparison of the Fe L_3 edge spectra at 10 K after cooling the sample from 300 K and illumination with a green LED at 10 K.

population of multiplet states in the HS state closely spaced in energy² but could also be due to probing a different amount of molecules.

To get rid of the initial light exposure effect, the sample was heated to 300 K and then cooled to 10 K in the characterization chamber (Figure 3b). Two main features observed around 706.9 eV (HS) and 708.3 eV (LS) in the Fe L_3 edge at 10 K indicate a spin-state coexistence.^{2–4,31} Upon illumination of the sample for 20 min with the green LED at 10 K (Figure 3b), a complete HS state was observed, indicating the LIESST-mediated LS-to-HS switching of the LS fraction coexisting with the HS fraction before illumination. The higher intensity of the peaks at 10 K (as prepared) in comparison to the 300 K data (Figure 3a) and the light-illuminated spectrum (Figure 3b) indicates that either some of the molecules were damaged by the X-ray exposure or the measurement position was changed due to thermal expansion of the sample manipulator.

Thermal switching kinetics of the deposited complex at submonolayer coverage was studied in detail by measuring XAS spectra as a function of temperature. Panels a and b of Figure 4 show the temperature dependence of the intensity variation of the peaks at the Fe L_3 edge for a 10–300 K heat-cool cycle. Heating the sample from 10 to 300 K results in the occurrence of temperature-induced LS-to-HS switching with a maximum LS fraction of 43% observed at 80 K (inset of Figure 4a).

An incomplete temperature-induced HS-to-LS switching was observed upon cooling the sample from 300 to 10 K; LS fractions of 42% and 32% were observed at 40 and 10 K, respectively. The SOXIESST-mediated LS-to-HS switching, operative below 60 K, caused the decrease of the LS fraction at

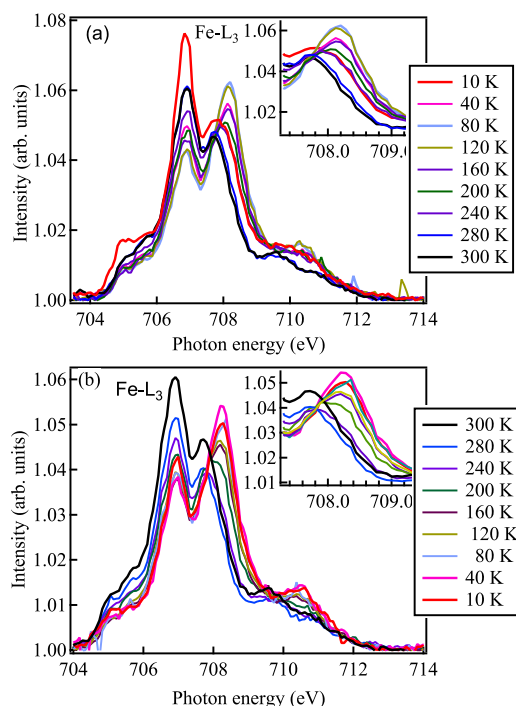


Figure 4. Fe L_3 spectra taken during heating (a) and cooling of the sample (b). The inset shows a close-up of the high-energy multiplet L_3 edge associated with the LS state.

10 K compared to the LS fraction observed at 40 K (inset of Figure 4b). Overall, an incomplete temperature-induced spin-state switching was observed for the submonolayer deposit of the complex on HOPG. Such an observation is in contrast to the complete spin-state switching observed in the bulk ($T_{1/2} = 197$ K) and in 10 nm thin films ($T_{1/2} = 177$ K) of the same complex.²¹ Thus, the molecule–HOPG substrate interactions hinder the temperature-induced SCO of the complex to a certain extent.

To elaborate the thermodynamic parameters associated with the spin-state switching in the submonolayer deposit of the complex on HOPG, the HS fractions calculated from the heating and cooling cycles have been fitted using a modified van't Hoff equation (1);² see Figure 5,

$$\gamma_{\text{HS}}(T) = x + (1 - x) \times [\exp(\Delta H/RT - \Delta S/R) + 1]^{-1} \quad (1)$$

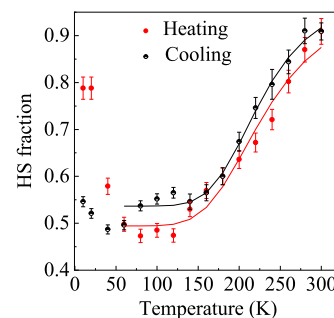


Figure 5. HS fraction obtained during cooling and heating of the sample. Solid lines show the fits to the data using eq 1. The HS fraction remained the same while heating up the sample from 10 to 20 K.

where ΔH and ΔS are the enthalpy and entropy difference, respectively, between the HS and LS states, R is the gas constant, and x is the remanent HS fraction. The data have been fitted in the range from 300 to 60 K to avoid the SOXIESST effect.

From the fits of Figure 5, $\Delta S = 43(5) \text{ J K}^{-1} \text{ mol}^{-1}$, $\Delta H = 10(1) \text{ kJ mol}^{-1}$, and $x = 0.49(1)$ were obtained for the heating branch. On the other hand, $\Delta S = 53(4) \text{ J K}^{-1} \text{ mol}^{-1}$, $\Delta H = 12(1) \text{ kJ mol}^{-1}$, and $x = 0.53(1)$ were obtained for the cooling branch. Using the relation $T_{1/2} = \Delta H/\Delta S$, 230 and 226 K were obtained for the heating and cooling branches, respectively. The thermodynamic parameters and $T_{1/2}$ are larger than the values $\Delta S = 38.7 \pm 7 \text{ J K}^{-1} \text{ mol}^{-1}$, $\Delta H = 5.7 \pm 1 \text{ kJ mol}^{-1}$, and $T_{1/2} = 148.5 \text{ K}$ found for 0.35 ML of the parent complex $[\text{Fe}(\text{H}_2\text{B}(\text{pz})_2)_2\text{-bipy}]$ deposited on HOPG (see Supporting Information of ref 5). Moreover, the $T_{1/2}$ values of the heating and cooling branches of the submonolayer deposit of $[\text{Fe}(\text{H}_2\text{B}(\text{pz})_2)_2\text{COOC}_{12}\text{H}_{25}\text{-bipy}]$ are also larger than the $T_{1/2}$ values reported for the complex $[\text{Fe}(\text{H}_2\text{B}(\text{pz})_2)_2\text{C}_{12}\text{-bipy}]$ in the bulk (197 K) and in 10 nm thin film (177 K).²¹ The values of $T_{1/2} = 195 \text{ K}$, $\Delta S = 82(2) \text{ J K}^{-1} \text{ mol}^{-1}$ and $\Delta H = 16(1) \text{ kJ mol}^{-1}$ and $T_{1/2} = 172 \text{ K}$, $\Delta S = 64(2) \text{ J K}^{-1} \text{ mol}^{-1}$ and $\Delta H = 11(1) \text{ kJ mol}^{-1}$ are obtained for bulk and 10 nm thin film, respectively, by fitting the data from ref 21 shown in Figure 1b with eq 1, using $x = 0$. These entropy and enthalpy values are larger than the ones for the HOPG-bound submonolayer sample in this study.

The locking of 50% of the molecules in the HS state is probably due to CH- π interactions between the methyl and methylene group and the HOPG substrate,³² which was also reported in the case of methyl groups attached to the parent compound.¹⁶ Theoretically, it has been reported that a mixed spin state is favored for surface-bound SCO complexes due to the interaction energy (epitaxial strain energy), which stabilizes a proportion of HS molecules at low temperatures.²² Although we cannot exclude fragmentation, it is unlikely that the complex is fragmented on HOPG when considering the stable nature of previously studied SCO complexes on HOPG.²⁻⁶ It is difficult to distinguish fragmentation by XAS if the absorption spectra of the fragments do not differ much.^{15,17}

The entropy difference between the HS and LS states arises as a consequence of the higher number of accessible vibrational states and the higher spin multiplicity associated with the HS state compared to the LS state. The value of ΔS can be better understood by examining in more detail the entropy change in the solid state. The main contribution arises from the electronic (ΔS_{elc}) and vibrational (ΔS_{vib}) entropy variations. Both ΔS_{elc} and ΔS_{vib} favor the HS state with only ΔS_{vib} being temperature-dependent and increasing at higher temperatures. In the ideal situation of an Fe(II) complex with octahedral symmetry, ΔS_{vib} ranges from 40 to 80 $\text{J K}^{-1} \text{ mol}^{-1}$ between 100 and 300 K compared to $\Delta S_{\text{elc}} = 13.38 \text{ J K}^{-1} \text{ mol}^{-1}$.³³ The value of $\Delta S = 53(4) \text{ J K}^{-1} \text{ mol}^{-1}$ for 0.4 ML of $[\text{Fe}(\text{H}_2\text{B}(\text{pz})_2)_2\text{COOC}_{12}\text{H}_{25}\text{-bipy}]$ is thus at the lower end of the range for the ideal octahedral Fe(II) complex.

Unlike the bulk behavior, the spin-state switching of the submonolayer of $[\text{Fe}(\text{H}_2\text{B}(\text{pz})_2)_2\text{COOC}_{12}\text{H}_{25}\text{-bipy}]$ on HOPG is associated with a hysteresis, which can be ascribed to the following factors: first, the differences in the LS-to-HS state transition between the cooling and heating branches below 60 K could be caused by the SOXIESST and LIESST effects, as discussed earlier. Second, the hysteretic behavior above 60 K could arise due to the lag in responding to the

change in sample surface temperature with respect to the temperature measured at the thermocouple. The observed hysteresis might be narrowed down (in future experiments) by further decreasing the temperature scan rate of the cooling branch.^{34,35} Not discussed in this frame are intermolecular interactions that may contribute to a hysteresis. However, such interactions are expected to have only a minor effect at the 0.4 ML coverage investigated here due to the large distance between the SCO complexes.

To investigate the role of molecule-HOPG substrate interactions on the LIESST-mediated LS-to-HS switching characteristics of $[\text{Fe}(\text{H}_2\text{B}(\text{pz})_2)_2\text{COOC}_{12}\text{H}_{25}\text{-bipy}]$, time-dependent XAS measurements were performed after illuminating the sample with the green LED at 10 K (Figure 6a). For

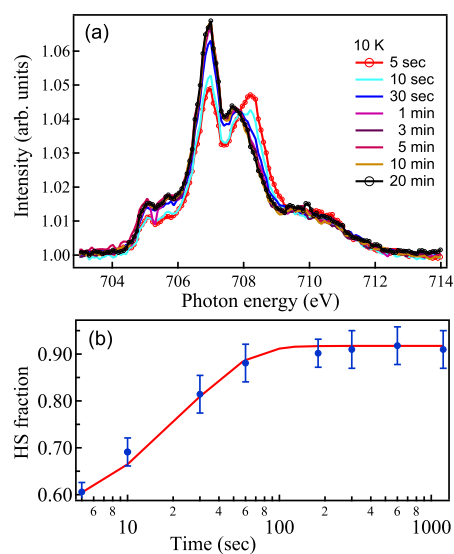


Figure 6. (a) Time-dependent XAS spectra obtained after successive illumination with green light at 10 K. (b) HS fraction versus $\log(t)$ plot. The vertical axis shows the HS fraction obtained from (a). The HS fraction normalized between 0 and 1 is used to fit the data, which results in a rate constant r of $0.043(2) \text{ s}^{-1}$.

those measurements, the sample was cooled from RT. A complete LIESST-mediated LS-to-HS switching occurred after 20 min of illumination. Since the relaxation of the HS molecules can be fast, depending on temperature, only the Fe L_3 edge was measured. Figure 6b shows the HS fraction as a function of illumination time. The obtained HS fraction between 0.59 and 0.92 was normalized and fitted to an exponential rate function, $1 - \exp(-r \times \text{time})$, where r is the rate constant, to quantify the LIESST. A rate of $r = 0.043(2) \text{ s}^{-1}$ is obtained from the fit. The obtained rate constant also includes the contribution from SOXIESST affecting the LS-to-HS spin-state switching below 60 K. Furthermore, the thermal relaxation of HS to LS contributes to the rate but is considered very slow at low temperatures as observed for the parent complex in ref 5. On the basis of a previous report detailing the SCO of the parent complex at different coverages on HOPG,⁵ we conclude that the main mechanism responsible for the LS-to-HS switching is LIESST.

In the last, we have performed temperature-dependent XAS studies in the 10-to-160-K range under constant illumination to quantify the kinetics by HS-LS switching rates. After performing XAS measurements in the 10 to 160 K heating and cooling cycle, the sample position was changed to minimize

the SOXIESST-induced LS-to-HS switching and to avoid radiation damage of the molecules. The change of the position of the beam spot on the sample resulted in a change of spectral intensity below 50 K while cooling, as can be seen in Figure 7a,b. The changing intensity of the Fe L₃ peak indicates a

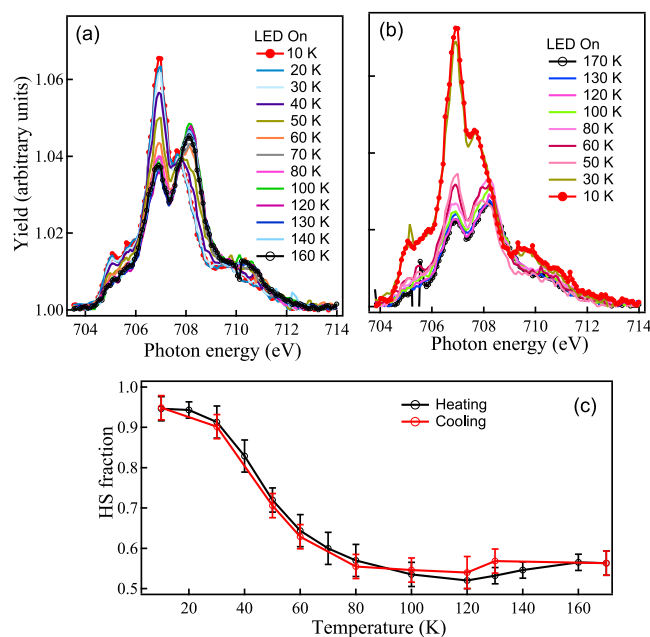


Figure 7. (a) XAS spectra obtained under illumination with green light, during heating (a) and cooling (b) of the sample. (c) Calculated HS fraction as a function of temperature extracted from (a), (b).

nonuniform distribution of the molecules. The beam position on the sample when obtaining the spectra while cooling from 170 to 50 K, as shown in Figure 7b, was relatively close to the upper edge of the sample where the coverage was a bit lower. The evolution of the HS fraction with temperature under illumination with green light is shown in Figure 7c. Approximately 50% of the complexes show spin-state switching (HS-to-LS) for heating and cooling cycles in the temperature range 160 to 10 K. Below 30 K, the spin state is dominated by the light-induced metastable HS state. Between 30 and 80 K, there is a rapid interconversion between HS and LS states. For temperatures ≥ 80 K, the HS fraction shows only small variations with a further increase in temperature, which indicates that almost all switchable HS-state molecules switched back to the LS state.

To extract the rate constant from Figure 7c, we have to consider the equilibrium of two phenomena. First, LS \rightarrow HS by LIESST where $d\gamma_{\text{HS}}/dt = r\gamma_{\text{LS}} = r(1 - \gamma_{\text{HS}})$ due to light illumination, which is independent of temperature, where r is the rate constant obtained from Figure 6b. The second is the HS \rightarrow LS thermal back-conversion, $d\gamma_{\text{HS}}/dt = -\alpha\gamma_{\text{HS}}$, where α is the rate constant as a function of temperature. In dynamic equilibrium between thermal back-conversion and LIESST, we get $\alpha(T) = r(1/\gamma_{\text{HS}} - 1)$. In the low-temperature region (< 30 K), the HS \rightarrow LS relaxation is very slow, which makes it difficult to accurately determine the rate. This is in accordance with an earlier study on the bulk parent molecule,³⁶ where thermal activation of the relaxation processes becomes more important in the temperature region ≥ 35 K. Above 120 K, the HS-fraction increase is attributed to the entropy-driven LS-to-HS conversion. Therefore, the rate of relaxation was evaluated

only in the temperature region $30 \text{ K} \leq T \leq 120 \text{ K}$. To calculate the activation energy (E_a) for the heating and cooling cycles, $\ln \alpha$ was plotted as a function of $1/T$ (Figure 8), which

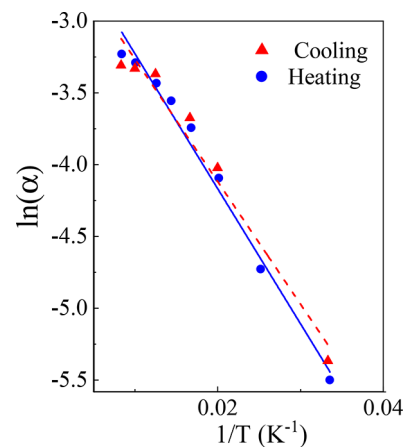


Figure 8. Rate constant ($\ln \alpha$) versus inverse temperature in an Arrhenius plot for the heating and cooling cycles. The straight lines show the fits of the data.

represents an Arrhenius plot. In this temperature region, the Arrhenius plot gives some apparent straight lines, confirming the assumption of a thermally activated process. Values of the pre-exponential factor equal to $0.10(1) \text{ s}^{-1}$ and of $E_a = 787(32)$ and $709(56) \text{ J/mol}$ were obtained for heating and cooling cycles, respectively. The value of E_a is around 4 times smaller than in the parent bulk material,³⁶ indicating a less stable light- and temperature-induced HS state on the HOPG substrate by faster thermal backconversion. It is worth emphasizing that even with the addition of $-\text{COOC}_{12}\text{H}_{25}$, 50% of the complex is still showing SCO properties. This indicates that the hydrophobic interactions between the hydrophobic tail and HOPG do not hinder the SCO behavior of the molecules as much as methyl groups.¹⁶

CONCLUSION

The presented temperature-dependent XAS studies indicate a clear role of the surface in partially blocking the temperature-induced spin-state switching of a 0.4 ML coverage of $[\text{Fe}(\text{H}_2\text{B}(\text{pz})_2)_2\text{COOC}_{12}\text{H}_{25}\text{-bipy}]$ on HOPG. Purely thermal SCO behavior was observed only from 50% of the molecules, while the remaining 50% are in a temperature-independent HS state. The light-induced LS-to-HS switching of the molecules was observed at low temperatures upon irradiation of the sample with green light. Temperature-dependent XAS measurements, from 10 to 160 K in both heating and cooling conditions, under continuous light irradiation confirm that 50% of the complexes switch on HOPG. Overall, the observation of light-induced spin-state switching of a functional and sublimable SCO complex $[\text{Fe}(\text{H}_2\text{B}(\text{pz})_2)_2\text{COOC}_{12}\text{H}_{25}\text{-bipy}]$ reported in this study is encouraging to consider vacuum-sublimable SCO complexes for the realization of light-addressable SCO-based switching and memory architectures. The results presented in the study furthermore highlight the importance of light-induced switching compared to purely thermally driven SCO transitions. The HS-to-LS transition of the HOPG-bound films presented in this study is temporally slow; complete switching occurred after around 20 min of light irradiation. Faster spin-state

switching dynamics can be realized by designing appropriate sublimable iron(II) complexes, adopting molecular engineering strategies.

AUTHOR INFORMATION

Corresponding Authors

Sangeeta Thakur – Institut für Experimentalphysik, Freie Universität Berlin, 14195 Berlin, Germany; orcid.org/0000-0003-4879-5650; Email: sangeeta.thakur@fu-berlin.de

Kuppusamy Senthil Kumar – Institute of Nanotechnology, Karlsruhe Institute of Technology (KIT), 76344 Eggenstein-Leopoldshafen, Germany; Institut de Physique et Chimie des Matériaux de Strasbourg (IPCMS), CNRS-Université de Strasbourg, 67034 Strasbourg cedex 2, France; orcid.org/0000-0002-1501-7759; Email: senthil.kuppusamy2@kit.edu

Mario Ruben – Institute of Nanotechnology, Karlsruhe Institute of Technology (KIT), 76344 Eggenstein-Leopoldshafen, Germany; Institute for Quantum Materials and Technologies (IQMT), Karlsruhe Institute of Technology (KIT), 76344 Eggenstein-Leopoldshafen, Germany; Institut de Science et d'Ingénierie Supramoléculaire (ISIS), Université de Strasbourg (Unistra), F-67000 Strasbourg, France; Email: mario.ruben@kit.edu

Wolfgang Kuch – Institut für Experimentalphysik, Freie Universität Berlin, 14195 Berlin, Germany; orcid.org/0000-0002-5764-4574; Email: kuch@physik.fu-berlin.de

Authors

Evangelos Golias – Institut für Experimentalphysik, Freie Universität Berlin, 14195 Berlin, Germany

Ivar Kumberg – Institut für Experimentalphysik, Freie Universität Berlin, 14195 Berlin, Germany

Rahil Hosseinifar – Institut für Experimentalphysik, Freie Universität Berlin, 14195 Berlin, Germany

Jorge Torres-Rodríguez – Institut für Experimentalphysik, Freie Universität Berlin, 14195 Berlin, Germany

Lalminthang Kipgen – Institut für Experimentalphysik, Freie Universität Berlin, 14195 Berlin, Germany

Christian Lotze – Institut für Experimentalphysik, Freie Universität Berlin, 14195 Berlin, Germany; orcid.org/0000-0001-6847-5676

Lucas M. Arruda – Institut für Experimentalphysik, Freie Universität Berlin, 14195 Berlin, Germany; orcid.org/0000-0003-3601-9793

Chen Luo – Helmholtz-Zentrum Berlin für Materialien und Energie, 12489 Berlin, Germany; Institute of Experimental Physics of Functional Spin Systems, Technical University Munich, 85748 Garching b. München, Germany

Florin Radu – Helmholtz-Zentrum Berlin für Materialien und Energie, 12489 Berlin, Germany

Complete contact information is available at: <https://pubs.acs.org/10.1021/acs.jpcc.1c02774>

Notes

The authors declare no competing financial interest.

ACKNOWLEDGMENTS

We gratefully acknowledge financial support by the BMBF through project VEKMag (BMBF 05K16KE3 and 05K19KEA). We thank the HZB for the allocation of synchrotron radiation beamtime and Kai Chen for support

during the beamtimes. M.R. thanks the grant agencies innovation FRC for financial support of the project “Self-assembly of spin-crossover (SCO) complexes on graphene”, and the DFG priority program 1928 “COORNETS” for generous support.

REFERENCES

- (1) Senthil Kumar, K.; Ruben, M. Emerging trends in spin crossover based functional materials and devices. *Coord. Chem. Rev.* **2017**, *346*, 176–205.
- (2) Bernien, M.; Naggert, H.; Arruda, L. M.; Kipgen, L.; Nickel, F.; Miguel, J.; Hermanns, C. F.; Krüger, A.; Krüger, D.; Schierle, E.; Weschke, E.; Tuzcek, F.; Kuch, W. Highly Efficient Thermal and Light-Induced Spin-State Switching of an Fe(II) Complex in Direct Contact with a Solid Surface. *ACS Nano* **2015**, *9*, 8960–8966.
- (3) Kipgen, L.; Bernien, M.; Nickel, F.; Naggert, H.; Britton, A. J.; Arruda, L. M.; Schierle, E.; Weschke, E.; Tuzcek, F.; Kuch, W. Soft-x-ray-induced spin-state switching of an adsorbed Fe(II) spin-crossover complex. *J. Phys.: Condens. Matter* **2017**, *29*, 394003.
- (4) Bernien, M.; Wiedemann, D.; Hermanns, C. F.; Krüger, A.; Rolf, D.; Kroener, W.; Müller, P.; Grohmann, A.; Kuch, W. Spin Crossover in a Vacuum-Deposited Submonolayer of a Molecular Iron(II) Complex. *J. Phys. Chem. Lett.* **2012**, *3*, 3431–3434.
- (5) Kipgen, L.; Bernien, M.; Ossinger, S.; Nickel, F.; Britton, A.; Arruda, L.; Naggert, H.; Luo, C.; Lotze, C.; Ryll, H.; Radu, F.; Schierle, E.; Weschke, E.; Tuzcek, F.; Kuch, W. Evolution of cooperativity in the spin transition of an iron(II) complex on a graphite surface. *Nat. Commun.* **2018**, *9*, 2984.
- (6) Ossinger, S.; Naggert, H.; Kipgen, L.; Jasper-Toennies, T.; Rai, A.; Rudnik, J.; Nickel, F.; Arruda, L. M.; Bernien, M.; Kuch, W.; Berndt, R.; Tuzcek, F. Vacuum-Evaporable Spin-Crossover Complexes in Direct Contact with a Solid Surface: Bismuth versus Gold. *J. Phys. Chem. C* **2017**, *121*, 1210–1219.
- (7) Gütllich, P.; Ksenofontov, V.; Gaspar, A. B. Pressure effect studies on spin crossover systems. *Coord. Chem. Rev.* **2005**, *249*, 1811–1829 presented at the 36th International Conference on Coordination Chemistry, Merida, Mexico, July 2004.
- (8) Zhang, L.; Tong, Y.; Kelai, M.; Bellec, A.; Lagoute, J.; Chacon, C.; Girard, Y.; Rousset, S.; Boillot, M.-L.; Rivière, E.; Mallah, T.; Otero, E.; Arrio, M.-A.; Sainctavit, P.; Repain, V. Anomalous Light-Induced Spin-State Switching for Iron(II) Spin-Crossover Molecules in Direct Contact with Metal Surfaces. *Angew. Chem., Int. Ed.* **2020**, *59*, 13341–13346.
- (9) Kahn, O.; Martinez, C. J. Spin-Transition Polymers: From Molecular Materials Toward Memory Devices. *Science* **1998**, *279*, 44–48.
- (10) Fert, A. Nobel Lecture: Origin, development, and future of spintronics. *Rev. Mod. Phys.* **2008**, *80*, 1517–1530.
- (11) Moth-Poulsen, K.; Bjørnholm, T. Molecular electronics with single molecules in solid-state devices. *Nat. Nanotechnol.* **2009**, *4*, 551–556.
- (12) Song, H.; Reed, M. A.; Lee, T. Single molecule electronic devices. *Adv. Mater.* **2011**, *23*, 1583–1608.
- (13) Prins, F.; Monrabal-Capilla, M.; Osorio, E. A.; Coronado, E.; van der Zant, H. S. J. Room-Temperature Electrical Addressing of a Bistable Spin-Crossover Molecular System. *Adv. Mater.* **2011**, *23*, 1545–1549.
- (14) Kumar, K. S.; Ruben, M. Sublimable Spin-Crossover Complexes: From Spin-State Switching to Molecular Devices. *Angew. Chem., Int. Ed.* **2021**, *60*, 7502–7521.
- (15) Gruber, M.; Berndt, R. Spin-Crossover Complexes in Direct Contact with Surfaces. *Magnetochemistry* **2020**, *6*, 35.
- (16) Ossinger, S.; Kipgen, L.; Naggert, H.; Bernien, M.; Britton, A. J.; Nickel, F.; Arruda, L. M.; Kumberg, I.; Engesser, T. A.; Golias, E.; Näther, C.; Tuzcek, F.; Kuch, W. Effect of ligand methylation on the spin-switching properties of surface-supported spin-crossover molecules. *J. Phys.: Condens. Matter* **2020**, *32*, 114003.

- (17) Rohlf, S.; Grunwald, J.; Jasper-Toennies, T.; Johannsen, S.; Diekmann, F.; Studniarek, M.; Berndt, R.; Tuzcek, F.; Rosnagel, K.; Gruber, M. Influence of Substrate Electronic Properties on the Integrity and Functionality of an Adsorbed Fe(II) Spin-Crossover Compound. *J. Phys. Chem. C* **2019**, *123*, 17774–17780.
- (18) Knaak, T.; González, C.; Dappe, Y. J.; Harzmann, G. D.; Brandl, T.; Mayor, M.; Berndt, R.; Gruber, M. Fragmentation and Distortion of Terpyridine-Based Spin-Crossover Complexes on Au(111). *J. Phys. Chem. C* **2019**, *123*, 4178–4185.
- (19) Gopakumar, T. G.; Bernien, M.; Naggert, H.; Matino, F.; Hermanns, C. F.; Bannwarth, A.; Mühlenberend, S.; Krüger, A.; Krüger, D.; Nickel, F.; Walter, W.; Berndt, R.; Kuch, W.; Tuzcek, F. Spin-crossover complex on Au(111): structural and electronic differences between mono- and multilayers. *Chem. - Eur. J.* **2013**, *19*, 15702–15709.
- (20) Poggini, L.; et al. Surface effects on a photochromic spin-crossover iron(ii) molecular switch adsorbed on highly oriented pyrolytic graphite. *Nanoscale* **2019**, *11*, 20006–20014.
- (21) Kumar, K. S.; Studniarek, M.; Heinrich, B.; Arabski, J.; Schmerber, G.; Bowen, M.; Boukari, S.; Beaurepaire, E.; Dreiser, J.; Ruben, M. Engineering On-Surface Spin Crossover: Spin-State Switching in a Self-Assembled Film of Vacuum-Sublimable Functional Molecule. *Adv. Mater.* **2018**, *30*, 1705416.
- (22) Fourmental, C.; et al. Importance of Epitaxial Strain at a Spin-Crossover Molecule–Metal Interface. *J. Phys. Chem. Lett.* **2019**, *10*, 4103–4109.
- (23) Takahashi, K.; Okai, M.; Mochida, T.; Sakurai, T.; Ohta, H.; Yamamoto, T.; Einaga, Y.; Shiota, Y.; Yoshizawa, K.; Konaka, H.; Sasaki, A. Contribution of Coulomb Interactions to a Two-Step Crystal Structure Phase Transformation Coupled with a Significant Change in Spin Crossover Behavior for a Series of Charged FeII Complexes from 2,6-Bis(2-methylthiazol-4-yl)pyridine. *Inorg. Chem.* **2018**, *57*, 1277–1287.
- (24) Noll, T.; Radu, F. *The Mechanics of the Vekmag Experiment*; 9th Mechanical Engineering Design of Synchrotron Radiation Equipment and Instrumentation; CERN, 2017; p WEPE38.
- (25) Outka, D. A.; Stöhr, J.; Jark, W.; Stevens, P.; Solomon, J.; Madix, R. J. Orientation and bond length of molecular oxygen on Ag(110) and Pt(111): A near-edge x-ray-absorption fine-structure study. *Phys. Rev. B: Condens. Matter Mater. Phys.* **1987**, *35*, 4119–4122.
- (26) Thompson, A. L.; Goeta, A. E.; Real, J. A.; Galet, A.; Muñoz, M. C. Thermal and light induced polymorphism in iron(II) spin crossover compounds. *Chem. Commun.* **2004**, 1390–1391.
- (27) Decurtins, S.; Gütllich, P.; Köhler, C.; Spiering, H.; Hauser, A. Light-induced excited spin state trapping in a transition-metal complex: The hexa-1-propyltetrazole-iron(II) tetrafluoroborate spin-crossover system. *Chem. Phys. Lett.* **1984**, *105*, 1–4.
- (28) Collison, D.; Garner, C. D.; McGrath, C. M.; Mosselmans, J. F. W.; Roper, M. D.; Seddon, J. M. W.; Sinn, E.; Young, N. A. Soft X-ray induced excited spin state trapping and soft X-ray photochemistry at the iron L_{2,3} edge in [Fe(phen)₂(NCS)₂] and [Fe(phen)₂(NCSe)₂]. *J. Chem. Soc., Dalton Trans. (1972-1999)* **1997**, 4371–4376.
- (29) Thole, B. T.; van der Laan, G. Branching ratio in x-ray absorption spectroscopy. *Phys. Rev. B: Condens. Matter Mater. Phys.* **1988**, *38*, 3158–3171.
- (30) Warner, B.; Oberg, J. C.; Gill, T. G.; El Hallak, F.; Hirjibehedin, C. F.; Serri, M.; Heutz, S.; Arrio, M.-A.; Sainctavit, P.; Mannini, M.; Poneti, G.; Sessoli, R.; Rosa, P. Temperature- and Light-Induced Spin Crossover Observed by X-ray Spectroscopy on Isolated Fe(II) Complexes on Gold. *J. Phys. Chem. Lett.* **2013**, *4*, 1546–1552.
- (31) Cartier dit Moulin, C.; Rudolf, P.; Flank, A. M.; Chen, C. T. Spin transition evidenced by soft x-ray absorption spectroscopy. *J. Phys. Chem.* **1992**, *96*, 6196–6198.
- (32) Karthikeyan, S.; Ramanathan, V.; Mishra, B. K. Influence of the Substituents on the CH... π Interaction: Benzene–Methane Complex. *J. Phys. Chem. A* **2013**, *117*, 6687–6694.
- (33) Nicolazzi, W.; Bousseksou, A. Thermodynamical aspects of the spin crossover phenomenon. *C. R. Chim.* **2018**, *21*, 1060–1074. Spin crossover phenomenon/Phénomène de transition de spin.
- (34) Kulmaczewski, R.; Olgúin, J.; Kitchen, J. A.; Feltham, H. L. C.; Jameson, G. N. L.; Tallon, J. L.; Brooker, S. Remarkable Scan Rate Dependence for a Highly Constrained Dinuclear Iron(II) Spin Crossover Complex with a Wide Thermal Hysteresis Loop. *J. Am. Chem. Soc.* **2014**, *136*, 878–881.
- (35) Brooker, S. Spin crossover with thermal hysteresis: practicalities and lessons learnt. *Chem. Soc. Rev.* **2015**, *44*, 2880–2892.
- (36) Moliner, N.; Salmon, L.; Capes, L.; Muñoz, M. C.; Létard, J.-F.; Bousseksou, A.; Tuchagues, J.-P.; McGarvey, J. J.; Dennis, A. C.; Castro, M.; Burriel, R.; Real, J. A. Thermal and Optical Switching of Molecular Spin States in the [FeL[H₂B(pz)₂]₂] Spin-Crossover System (L = bpy, phen). *J. Phys. Chem. B* **2002**, *106*, 4276–4283.